Applied Surface Science 255 (2009) 6097–6102

Contents lists available at ScienceDirect

Applied Surface Science

journal homepage: www.elsevier.com/locate/apsusc

Dislocation evolution in titanium during surface severe plastic deformation

Ming Wen [a,b], Gang Liu [c], Jian-feng Gu [d], Wei-ming Guan [a], Jian Lu [e,*]

[a] Kunming Institute of Precious Metals, Kunming, 650106, People's Republic of China
[b] Shenyang National Laboratory for Materials Science, Institute of Metals Research, Chinese Academy of Sciences, Shenyang, 110016, People's Republic of China
[c] Research Institute, Northeastern University, Shenyang, Liaoning, 110004, People's Republic of China
[d] School of Materials Science and Engineering, Shanghai Jiao Tong University, Shanghai, 200240, People's Republic of China
[e] Mechanical Engineering Department, The Hong Kong Polytechnic University, Hong Kong, China

ARTICLE INFO

Article history:
Received 2 April 2008
Received in revised form 23 December 2008
Accepted 19 January 2009
Available online 9 March 2009

PACS:
61.46.Hk
81.05.Bx

Keywords:
SMAT
Titanium
Dislocation
Dynamic recrystallization

ABSTRACT

Surface mechanical attrition treatment (SMAT) is an innovative technique which can produce nanocrystalline (nc) layers of several tens of micrometers thickness on surfaces of metallic materials. In this work, the grade structures of commercially pure titanium (CP Ti) processed by SMAT was studied intensively, and the microstructure observations indicated that the dislocation evolution could be separated into three steps: (1) formation of dislocation tangles; (2) formation of dislocation bands; and (3) dynamic recrystallization of dislocation bands until the formation of nc Ti.

1. Introduction

The use of titanium and its alloys in biomedical field has become a well established area due to their lower Young modulus, superior biocompatibility and enhanced corrosion resistance when compared to more conventional stainless steels and cobalt-based alloys [1–3]. The commercially pure titanium (CP Ti) is chemically inert and biologically more compatible than Ti–6Al–4 V, but coarse-grained (CG) Ti has low wear and abrasion resistance because of its low hardness [3]. Nanocrystalline (nc) and ultrafine-grained (UFG) materials have exhibited many novel properties such as high strength and hardness, as well as excellent tribological properties relative to their CG counterparts [4–6]. Due to the various limitations of present methods, preparation of ideal bulk nanocrystalline samples (free of contamination and porosity, bulk in size, uniform and small grain size) is still a challenge to materials scientists [7]. In fact, most failures of materials occurring on surfaces (fatigue fracture, fretting fatigue, wear and corrosion etc.) are very sensitive to the surface structure and properties, so that surface-optimization may effectively enhance the overall properties of materials. As concerned with the superior properties of nc materials, Lu et al. put forward that if a nc layer could be generated on a material surface, the global properties and behaviors will be greatly improved [8,9]. Surface mechanical attrition treatment (SMAT), an effective way to realize surface self-nanocrystallization on metallic materials without changing the chemical compositions, was proposed based on the above idea, and has already been realized in many metals and alloys such as Fe, AISI 304 stainless steel, Al-alloy, Cu, Mg-alloy, and Ti etc. [7,10–14].

In fact, SMAT could harmoniously be combined with other methods (hybrid SMAT) to produce functionally gradient materials by means of nanostructure-selective reaction due to the much enhanced atomic diffusivity and chemical reactivity of the nanostructured surface layer. Our previous investigations have revealed that [15–17]: (1) after treatment with hydrogen peroxide at room temperature (25 °C), nanoporous titania appeared on the SMAT Ti surface while CG Ti only showed intergranular corrosion. And the nanoporous structure could be retained even after calcination at 600 °C suggesting a good thermal stability; (2) after treatment with H_2O_2/HCl at 80 °C for 15 min and further calcination at 400 °C for 1 h, the SMAT Ti shows a high bioactivity which can be attributed to the unique structure on its surface, including the nanocrystalline anatase, negative surface charge, and the mesoporous structure.

The nanostructure formation mechanism of Ti (SMAT) was studied by Zhu et al. [14], but the dislocations evolution has not yet

* Corresponding author. Tel.: +852 27666665; fax: +852 2365 4703.
E-mail address: mmmelu@inet.polyu.edu.hk (J. Lu).

0169-4332/$ – see front matter © 2009 Elsevier B.V. All rights reserved.
doi:10.1016/j.apsusc.2009.01.048

been observed in details and dynamic recrystallization was only assumed just by the observation that no dislocations were found on the top of the surface layer (high-resolution TEM). In this work, the dislocation evolution in Ti (SMAT) was studied extensively and dynamic recrystallization was found directly which is important both from academic and applied points of view. By the way, since we focused on the dislocation evolution in the present study, the deformation twins and their interaction are out of scope and are only depicted briefly when necessary.

2. Experimental

The material used in this study was a CP Ti plate with the chemical composition (wt%): 0.10 Fe, 0.01 Si, 0.16 O, 0.014 N, 0.004 H, 0.022 C, 0.23 Al and balance Ti. The plate was annealed in an argon atmosphere at 740 °C for 2 h, and then air-cooled, obtaining equiaxed grains with the average size of 30 μm. The SMAT set-up had been described in detail elsewhere [8,9]. The key point of SMAT is to introduce a large amount of defects and/or interfaces into the surface layer by repeated multidirectional impacts at high strain rate over a short period of time, so that the crystallinity of the entire sample surface can be transformed from coarse grained into nanometer scale progressively. In this study, the vibration frequency of the system was 50 Hz, stainless steel balls with the diameter of 8 mm were selected, and the samples were treated in vacuum for 60 min at room temperature. TEM images and the corresponding selected area electron diffraction (SAED) were obtained by using a JEOL 2010 TEM with an accelerating voltage of 200 KV. The TEM specimens of different layers were obtained by polishing the corresponding layer until the thickness was about 30 μm, and followed by a single jet-polishing (coated the corresponding depth by glue) with electrolyte of 30 ml perchloric acid, 175 ml butyl alcohol and 300 ml methanol at −30 °C.

3. Results

The typical microstructure features at the depth of 300 μm from the treated surface were dislocation tangles and deformation twins. Fig. 1 shows dislocation tangles are tangled with each other in a complex way, and the corresponding selected area electron diffraction shows no misorientions inside the tangles. So twinning and slipping occur concurrently in the beginning of SMAT making the deformation of Ti proceed continuously.

Fig. 2 shows the bright field image of SMAT Ti at the depth of 250 μm from the treated surface. As the elastic strain (such as the stored elastic energy or local effective stress, etc.) and strain rate increase, the irregular dislocation tangles (Fig. 1) change to dislocation lamellae in which distribution of dislocation is approximate homogeneous, judging by the similarity of the contours. The width of dislocation lamellae is about 200–600 nm. The boundaries approximately parallel to $\{1\,0\,\bar{1}\,0\}$ indicating that, at the beginning of deformation, dislocation glide first gets activated in the predominant slip system of prismatic slip $\{1\,0\,\bar{1}\,0\}\langle 1\,1\,\bar{2}\,0\rangle$. The dislocation tangles' intersections with twins are also found at this depth and twin boundaries curve accordingly.

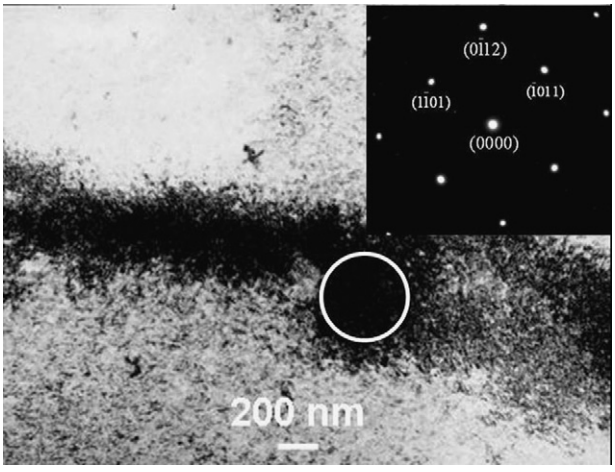

Fig. 1. Dislocation tangles of SMAT Ti at the depth of 300 μm from treated surface. The SAED is taken from the white ring.

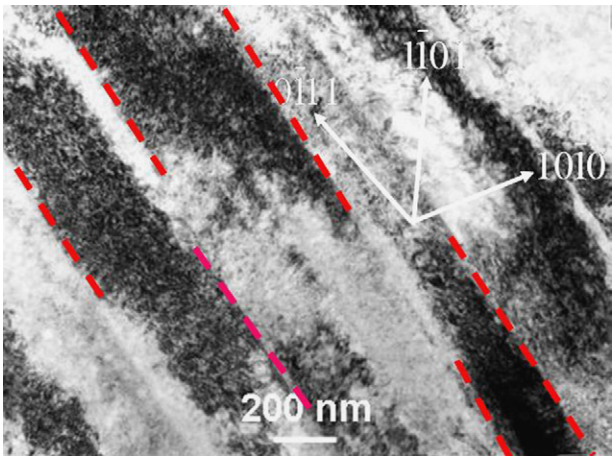

Fig. 2. Bright field images of SMAT Ti at the depth of 250 μm from treated surface.

When the depth reaches 200 μm from the treated surface, the deformation twins vanish and the dislocation lamellae evolve into subgrain boundaries with evident, but low misorientations (Fig. 3a). The length of subgrains is about several micrometers, and the width becomes narrower (150–350 nm). The boundaries are composed of dislocation tangles (D1 and D2) and subboundaries (S1, S2 and S3). For example, the misorientation of S1 is about 2.6° as shown in SAED inserted. Some boundaries deviate from $\{1\,0\,\bar{1}\,0\}$ which further confirms that basal slip and pyramidal slip could be activated when the strain is high enough. The boundaries form by the accumulating, annihilating and rearranging of dislocations. Some boundaries are concurrently composed of dislocation tangles and subboundaries suggesting that the dislocation tangles are changing into subboundaries with increasing strain and strain rate (Fig. 3b). It should be illuminated that, for their higher latent energy, subboundaries could be the prior nucleation sites of new subgrains. For instance, a new subgrain with the shape of an isosceles triangle forms in the triple junctions, as indicated by a white ring in Fig. 3a. The lamellae subgrains were also found during the SMAT procedures of pure Fe and Al alloy [7,10], resulting from the crystallographic slip on a dominant slip system and the followed propagation by multiple or cross slips because of stress concentration. With an increase of strain at this depth, the intersections of subboundaries become more and more frequent and thus smaller ultrafine grains form among these subboundaries.

Fig. 4 shows the bright field image of SMAT Ti at the depth of 180 μm from the treated surface. From Fig. 4a (number 1–8 inserted are eight adjacent subgrains), it can be seen that the typical microstructures at this depth are subgrains with low dislocation density. The width of subgrains is 60–280 nm and the SAED shows some brilliant spots as well as some small arcs indicating the existence of high angle misorientations among the subgrains. For example, as indicated by the white ring in Fig. 4b, the misorientation between the subgrain and surrounding is about 11.8°, suggesting the transition state from low to high angle grain boundary at this depth.

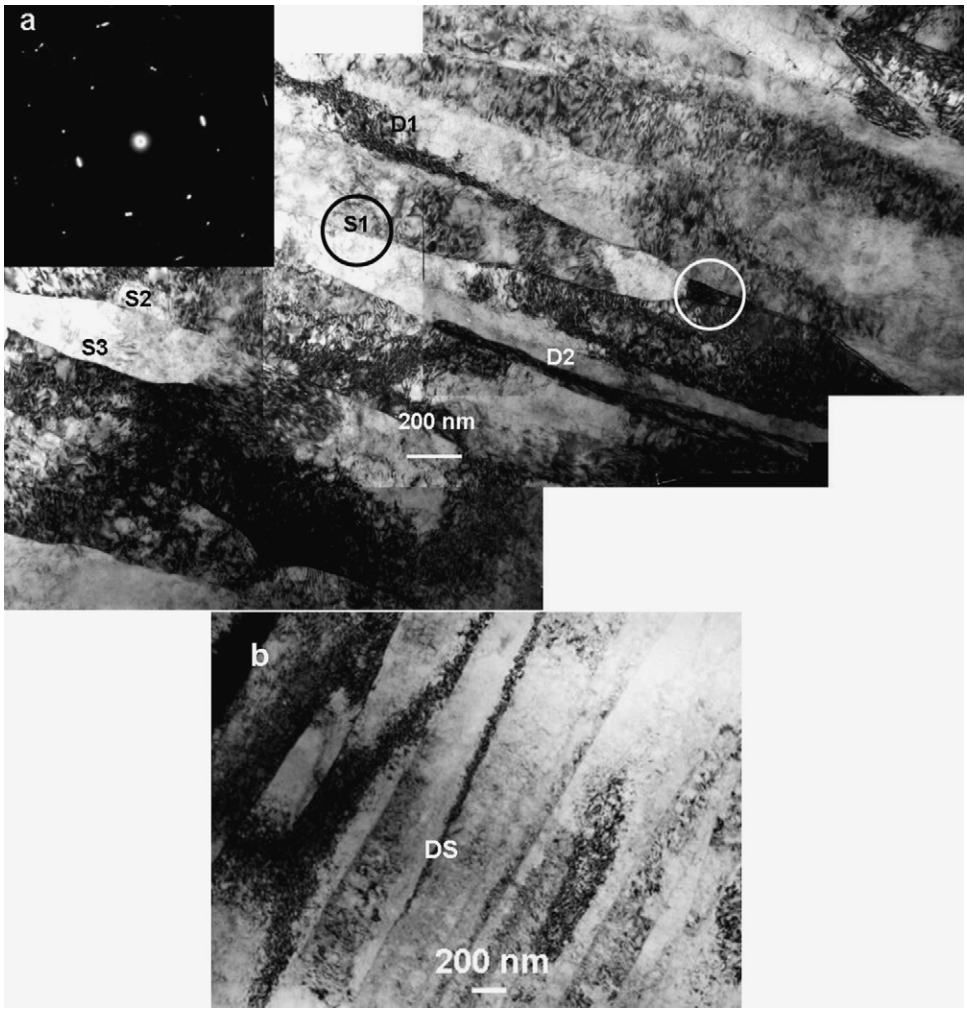

Fig. 3. Bright field images of SMAT Ti at the depth of 200 μm from treated surface. In (a) S: subboundaries, D: dislocation tangles, and the SAED inserted is taken from S1; (b) DS: the transition state from dislocation tangles to subboundaries.

At the depth of 150 μm from the treated surface, as shown in Fig. 5a, the subgrain with low dislocation density changes into band structure with high dislocation density (dislocation bands) and the width of which is about 40–150 nm. The dislocation bands are composed of two substructures as shown in Fig. 5b: (1) the SAED inserted indicates that the white ring area is still composed by several subgrains, and the dislocation bands could be further refined with increasing strain; and (2) the parallel, long black and gray bands which named banded-contrast image (BCI) (marked by white arrows in the left of Fig. 5b), and such images were formed by the strain fields of high-density dislocations. When such dislocations, approximately parallel to each other and possibly with the same Burgers vector, are oriented to a certain angle to the electron beam, their strain fields, or the interaction of their strain fields, will generate BCI [18].

When the depth decreases to 100 μm from the treated surface, as shown in Fig. 6, some of the dislocation bands gradually change into equiaxed subgrains gradually (marked by the white arrows). Dense dislocations still exist in grain

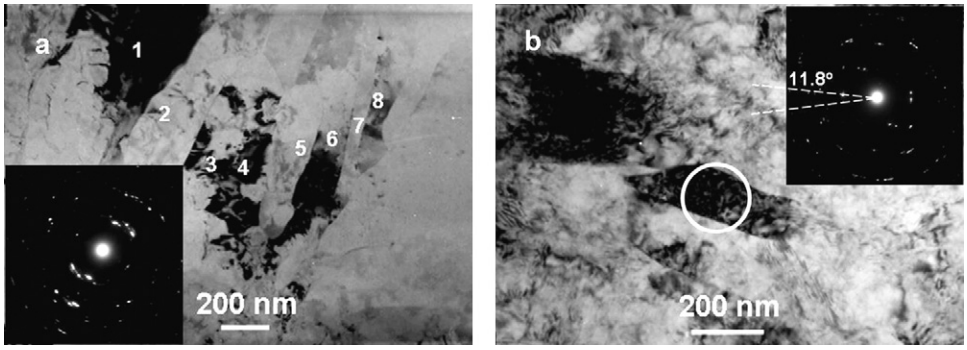

Fig. 4. TEM observations of the microstructure at about 180 μm deep from treated surface of SMAT Ti (a) bright field image and corresponding SAED; (b) the SAED inserted corresponding to the white ring.

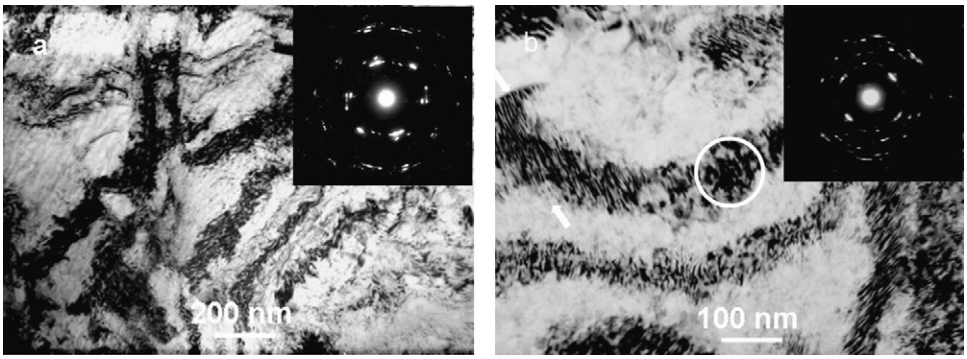

Fig. 5. (a) TEM observations of the microstructure at about 150 μm deep from treated surface of SMAT Ti; (b) high magnification image of dislocation bands. The SAED inserted correspond to the white ring and the banded-contrast image is indicated by white arrows.

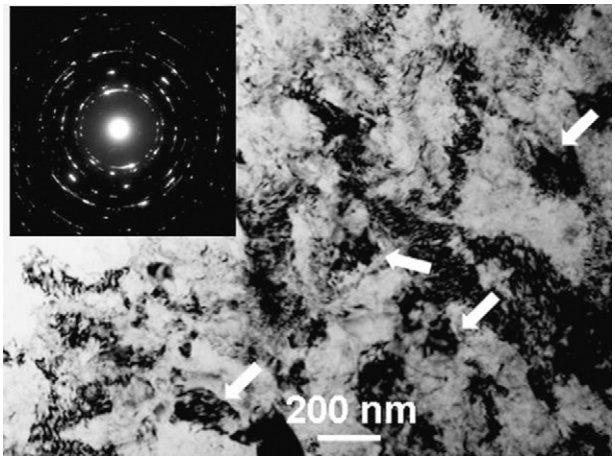

Fig. 6. Bright field images of SMAT Ti at the depth of 100 μm from treated surface.

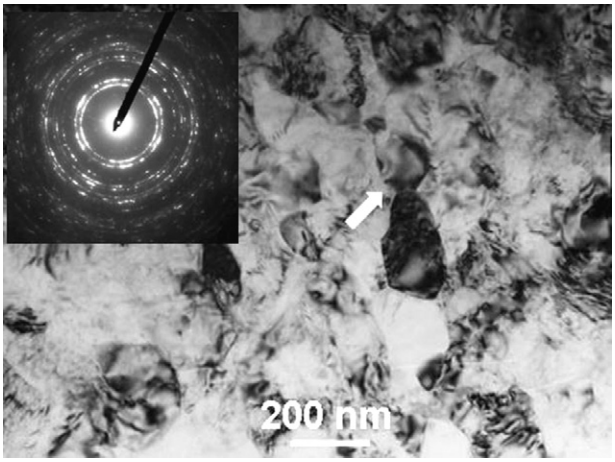

Fig. 7. Bright field images of SMAT Ti at the depth of 60 μm from treated surface.

interior, and the corresponding SAED shows discontinuous rings pattern suggesting coexistence of both grains and subgrains.

As the depth achieves 60 μm from the treated surface, the shape of subgrains becomes more regular (Fig. 7). As shown by the white arrow, two adjacent subgrains are in the progress of detaching from each other suggesting the existence of subgrains. The grain size varies from 100 to 600 nm, and the average grain size is about 250 nm by number-averaging the diameters of 180 grains.

Fig. 8a shows bright field TEM images of nc Ti at about 15 μm below the top surface. The grains are mostly equiaxed, and random orientations, as confirmed by the uniform ring pattern of the SAED. Higher magnification in Fig. 8b shows that a considerable number of dislocations still exist in the grains and grain boundaries, which may accommodate a high density of strain energy. The grain size distribution inserted was measured from a number of bright field and dark field TEM images by number-averaging the diameters of 160 grains. The grain size varies from 15 to 300 nm, and the average grain size is 103 nm.

4. Discussion

The hcp Ti has an axial ration of $c/a = 1.587$ (lower than the ideal $c/a = 1.633$), and is strongly plastically anisotropic [19]. With c/a ratio less than the ideal value, the lattice resistance for prism planes is lower than that for basal and pyramidal planes, hence the most common slip modes are in the sequence of

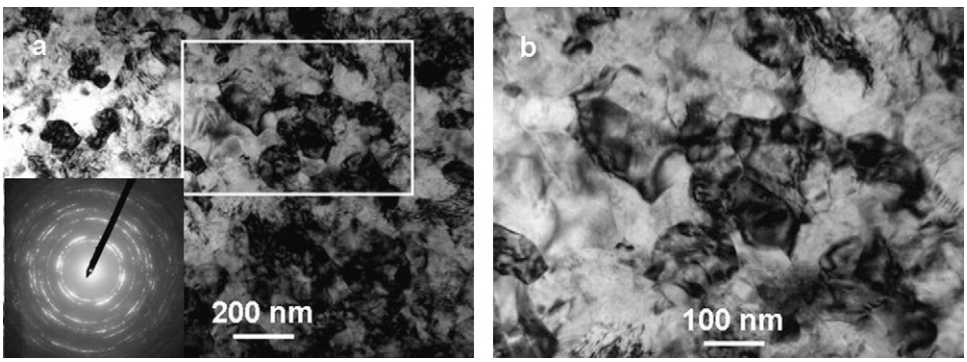

Fig. 8. (a) Bright field images of SMAT Ti at the depth of 15 μm from treated surface; (b) the higher magnification of the square in (a).

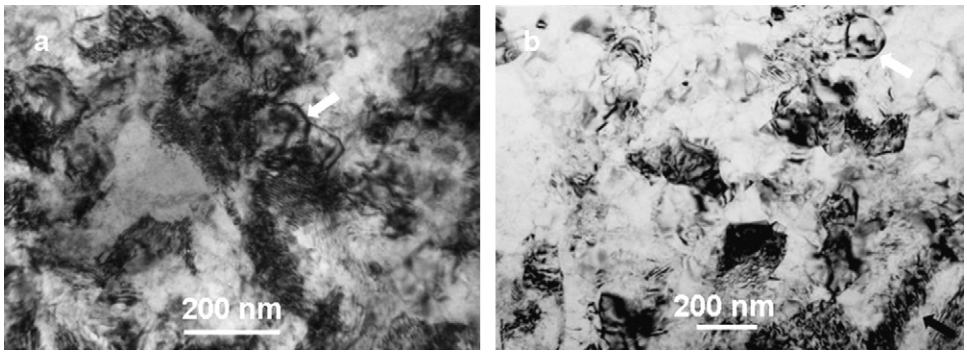

Fig. 9. Formation of strain-free ultrafine grains through dynamic recrystallization (a) the initial state; (b) the later state.

$\{1\,0\,\bar{1}\,0\}$, $\{1\,0\,\bar{1}\,1\}$ and $\{0\,0\,0\,1\}$ planes with $\langle 11\bar{2}0\rangle$ as the slip direction. However, five independent slip systems are required for a polycrystalline material to accommodate an arbitrary plastic strain, and thus the operations of twin systems are necessary in order to maintain the deformation compatibility since only four independent slip systems exist in Ti [20]. Twinning could not accommodate a huge amount of deformation due to the fact that the atomic displacement by twin is less than one inter-atomic distance. For example, Chichili et al. found that the plastic deformation due to twinning is less than 0.2% at low strain and strain rates [20]. In present study, we also found the same results, i.e., the deformation is mainly due to dislocation motion at the depth far from the treated surface. While moving in some slip planes, dislocations will curve when meeting some obstacles such as forest dislocations and the dislocation densities there will increase accordingly making dislocation tangles come into being. The deformation twinning can convert a large number of grains into a twin orientation whenever dislocation motion is restricted, and make dislocation slip again by the activating of other favorably oriented slip systems. When the strain attains a certain level, i.e., the dislocation density achieves some critical value, these dislocation will be annihilated and rearranged into ordered array (Fig. 2). The dislocation density in ordered arrays is still very high by the extinction contours meaning the strain in tangles is not high enough to completely activate dislocations. As the local elastic strain further increases, dislocation gliding, accumulation, interaction, tangle and spatial rearrangement to subdivide the origin grains into subgrains and no twins are found at this depth (Fig. 3). Zhu et al. also found that no twins exist in the ECAP procedure of Ti when the grain was refined to ultrafine grain regime [18]. Grain boundaries such as the triple junction could be the prior nucleation place of new subgrains due to the higher latent energy (Fig. 3a). With the gradual increasing of strain and strain rate, the width of subgrain becomes smaller and smaller (Fig. 4), and subgrains turn into dislocation bands (Fig. 5). Finally, the dislocation bands change into equiaxed subgrain by the dynamic recrystallization (DRX). As shown in Fig. 9a, two ultrafine grains with sharp grain boundaries form in the boundaries of a dislocation bands. It is commonly observed that deformation textures sharpen within the prior deformation textures are obtained through recovery [21]. As indicated by the white arrows in Fig. 9b, a strain-free ultrafine grain forms just over the site in Fig. 9a. It is well known that recrystallization will proceed by migration of the new grain boundaries into the deformed matrix leaving behind what are commonly known as strain-free grains. The migration is driven by the energy gradient across the boundary due to the presence of the deformed structure on one side and the recrystallized structure on the other [21]. Two type of DRX based on the operating structural mechanisms that result in new grain development are discontinuous DRX and continuous DRX. The new grain evolution in materials with low to medium stacking fault energy (SFE) is often associated with the discontinuous DRX, while continuous DRX is responsible for the materials with high SFE [22]. The new grain development in continuous DRX is a result of the gradual increase of misorientation between the subgrains that are caused by the continuous plastic deformation. As concerned with the very high SFE of Ti ($>300\ \mathrm{mJ/m^2}$) [23] and dislocation evolution during SMAT, it can be concluded that continuous DRX could take place in this procedure. In a word, the DRX processes result in a progressive accumulation of boundary misorientation, and finally lead to a gradual transition of boundaries character until the formation of high angle grain boundaries. In fact, the increased prior deformation may cause the continuous DRX to occur in a more uniform manner [21]. During SMAT, as the strain and strain rate increase with decreased distance from the treated surface, continuous recrystallization will initiate when the dislocation density achieves a critical value and then pervade through the material. Although DRX usually proceeds in the hot-working state, recently, Wang et al. also found DRX even at low temperature during the cold rolling of Cu at cryogenic temperature [24]. They believed that DRX could be triggered even at low temperature when a critical strain, ε_c, is reached. Zhang et al. also found DRX phenomena during the cryomilling of nc Zn powder [25]. During SMAT at room temperature, dense dislocation areas with high curvatures near surface are easily formed and store enough energy to trigger the initiation and propagation of DRX. It is commonly believed that the nucleation of DRX happens in certain locations of the deformed microstructure, particularly in deformation inhomogeneities like shear bands or microbands which contains high dislocation density. As with the decrease distance from the treated surface, new dislocation structure will form in refined subgrains and grains, suggesting that grain subdivision is conducted on a finer and finer scale by the above mechanism. Finally, the grain size will be invariable and achieve a stabilized grain size until dislocation multiplication rate is balanced with the annihilation rate. At the same time, the subgrain rotation will be promoted to high angle grain boundaries due to the multi-directional loading and high strain rates near surface.

5. Conclusion

A nanocrystalline surface layer was produced on a CP Ti by means of SMAT. Microstructure observations indicated that dislocation evolution could be separated into three steps: (1) formation of dislocation tangles; (2) formation of dislocation bands; and (3) dynamic recrystallization of dislocation bands until the formation of nc Ti.

Acknowledgements

This work was supported by NSFC (Grant No. 50431010), MOST of China (Grant No.2005CB623604), the Research Grant Council of the Hong Kong SAR under the project PolyU 5189/07E(GRF), the Hong Kong Polytechnic University (Grant No. BB90), and Yunnan NSF (Grant No. 2008CD201). In particular, one of the author (Ming Wen) would thank the reviewer and Prof. Li-yong Zhang for their careful reading this manuscript and valuabe criticisms to improve this manuscript.

References

[1] T. Kokubo, H.M. Kim, M. Kawashita, T. Nakamura, J. Mater. Sci.- Mater. Med. 15 (2004) 99–107.
[2] M. Long, H.J. Rack, Biomaterials 19 (1998) 1621–1639.
[3] X.Y. Liu, P.K. Chu, C.X. Ding, Mater. Sci. Eng. R. 47 (2004) 49–121.
[4] H. Gleiter, Acta Mater. 48 (2000) 1–29.
[5] K.S. Kumar, H. Van Swygenhoven, S. Suresh, Acta Mater. 51 (2003) 5743–5774.
[6] M.A. Meyers, A. Mishra, D.J. Benson, Prog. Mater. Sci. 51 (2006) 427–556.
[7] N.R. Tao, Z.B. Wang, W.P. Tong, M.L. Sui, J. Lu, K. Lu, Acta Mater. 50 (2002) 4603–4616.
[8] K. Lu, J. Lu, J. Mater. Sci. Technol. 15 (1999) 193–197.
[9] K. Lu, J. Lu, Mater. Sci. Eng. A 375–377 (2004) 38–45.
[10] X. Wu, N. Tao, Y. Hong, B. Xu, J. Lu, K. Lu, Acta Mater. 50 (2002) 2075–2084.
[11] H.W. Zhang, Z.K. Hei, G. Liu, J. Lu, K. Lu, Acta Mater. 51 (2003) 1871–1881.
[12] K. Wang, N.R. Tao, G. Liu, J. Lu, K. Lu, Acta Mater. 54 (2006) 5281–5291.
[13] H.Q. Sun, Y.N. Shi, M.X. Zhang, K. Lu, Acta Mater. 55 (2007) 975–982.
[14] K.Y. Zhu, A. Vassel, F. Brisset, K. Lu, J. Lu, Acta Mater. 52 (2004) 4101–4110.
[15] M. Wen, J.F. Gu, G. Liu, Z.B. Wang, J. Lu, Surf. Coat. Technol. 201 (2007) 6285–6289.
[16] M. Wen, J.F. Gu, G. Liu, Z.B. Wang, J. Lu, Cryst. Growth Des. 7 (2007) 2400–2403.
[17] M. Wen, J.F. Gu, G. Liu, Z.B. Wang, J. Lu, Appl. Surf. Sci. 254 (2008) 2905–2910.
[18] Y.T. Zhu, J.Y. Huang, J. Gubicza, T. Ungár, Y.M. Wang, E. Ma, R.Z. Valiev, J. Mater. Res. 18 (2003) 1908–1917.
[19] S. Nemat-Nasser, W.G. Guo, J.Y. Cheng, Acta Mater. 47 (1999) 3705–3720.
[20] D.R. Chichili, K.T. Ramesh, K.J. Hemker, Acta Mater. 46 (1998) 1025–1043.
[21] R.D. Doherty, D.A. Hughes, F.J. Humphreys, J.J. Jonas, D. Juul Jensen, M.E. Kassner, W.E. King, T.R. McNelley, H.J. McQueen, A.D. Rollett, Mater. Sci. Eng. A 238 (1997) 219–274.
[22] A. Belyakov, K. Tsuzaki, H. Hiura, T. Sakai, Acta Mater. 51 (2003) 847–861.
[23] D.J. Bacon, J.W. Martin, Philos. Mag. A 4 (1981) 883–900.
[24] Y.M. Wang, T. Jiao, E. Ma, Mater. Trans. 44 (2003) 1926–1934.
[25] X. Zhang, H. Wang, J. Narayan, C.C. Koch, Acta Mater. 49 (2001) 1319–1326.